Journal of Ovonic Research Vol. 17, No. 5, September - October 2021, p. 411 - 420

Electron irradiation effects on InP-based HEMTs with different gate widths

S. X. Sun[a,d,*], X. L. Fu[a], L. Wang[a], M. E[a], J. J. Yi[a], R. X. Yao[a], X. Y. Zheng[a], H. T. Wu[a], F Liu[a,d], Y. H. Zhong[b,*], Y. X. Li[b], P. Ding[c], Z. Jin[c]

[a] *Henan Provincial Key Laboratory of Smart Lighting,School of Information Engineering, Huanghuai University, Zhumadian 463000, China*

[b] *School of Physics and Microelectronics , Zhengzhou University, Zhengzhou 450001, China*

[c] *Institute of Microelectronics, Chinese Academy of Sciences, Beijing 100029, China*

[d] *Henan International Joint Laboratory of Behavior Optimization Control for Smart Robots, Zhumadian 463000, China*

In this paper, the influence of electron irradiation on DC and RF characteristics of InP-based HEMTs with different gate widths were studied by irradiation experiment. The results show that the value of channel current (I_{DS}) and transconductance (g_m) are decreased for device with different gate width after electron irradiation, which is mainly due to the reduction of mobility in the channel by the irradiation-induced defects. However, the carrier concentration in the channel has a little change. Compared with the device with 100 μm gate width, I_{DS} and g_m of the device with 40 μm gate width were decreased by 1.5% and 3%. Meanwhile, the forward gate current decreased due to the increase of series resistance of gate contact caused by electron irradiation. The interface defects induced by electron irradiation induced the increase of the reverse gate current. Additionally, the current gain cut-off frequency (f_T) and maximum oscillation frequency (f_{max}) were reduced by 19.8% and 10.9% for device with 40 μm gate width, and the f_T and f_{max} were only reduced by 7.1% and 8.2% for device with 100 μm gate width. The experimental results indicate that designing a reasonable structure is an effective method to enhance the radiation resistance in InP-based HEMTs, and this method can also be utilized in other semiconductor devices.

(Received May 25, 2021; Accepted September 3, 2021)

Keywords: InP-based HEMTs, Electron irradiation, Gate width, DC and RF characteristics

1. Introduction

Recently, millimeter-wave systems have rapidly emerged as a potential candidate for various attractive demands, such as 60 GHz short-range communication[1], 77 GHz automotive radar systems[2] and 94 GHz high-resolution imaging applications[3]. Due to ultra-fast carrier relaxation time, high breakdown field and high electron mobility, III-V compound semiconductor materials are widely used in a variety of high-frequency and high-power microelectronic

* Corresponding authors: zhongyinghui@zzu.edu.cn

devices[4-6]. Because of high carrier sheet density, high carrier peak drift velocity and low-field mobility in InGaAs channel, InAlAs/InGaAs InP-based high electron mobility transistors (HEMTs) demonstrate extremely excellent characteristics, such as high frequency, low noise figure, and superior gain performance and so on. Consequently, they have become competitive candidates for various millimeter-wave circuits [7-10] and space applications.

It is well-known that space equipments mostly operate at the van Allen radiation belt, which mainly include protons and electrons[11,12]. When semiconductor devices work in this environment, the radiation resistance of semiconductor devices must be established, due to the fact that performances of device will become deteriorated with irradiation time and dose[13,14]. Once the space radiation fluence reaches a certain value, the device will stop working, and leads to a failure the space equipment. Therefore, the irradiation degradation mechanism induced by proton or electron is of significant importance to prompt the pervasive application of InP-based HEMTs in space environment.

In the past decades, many researchers have done an immense amounts of research about the particles irradiation influence on HEMT by theory modeling and irradiation experiments[15-18]. Lv et al. and Liu et al. have made comprehensive analyses of proton irradiation on the output and transfer characteristics of AlGaN/GaN HEMTs, which indicated that the output and transfer characteristics were almost unchanged at low proton fluence, and with the increase of proton fluence, the characteristics got deteriorated more seriously[15,16]. Kimura et al. was studied the variation of Schottky gate characteristics InGaAs/GaAs HEMTs induced by electron irradiation. The results showed that the deterioration of the Schottky gate characteristics were attributed to the deep traps introduced at the gate metal and GaAs barrier layer[17]. However, these researches are mainly focused on GaN and GaAs based HEMTs and only a few papers are studied the irradiation effects on InP-based HEMT devices.

In this paper, the gate width dependence of changes in DC and RF characteristics of InP-based HEMTs exposed to the 1×10^{16} cm^{-2} electron dose and electron energy 1 MeV were investigated. The variation of electrical changes were analyzed, such as DC characteristics, RF characteristics and gate current characteristics. The results would provide a reliable theoretical guidance for anti-radiation of InP-based HEMTs.

2. Experiments

The heterostructures were fabricated by gas source molecular beam epitaxy (GSMBE) on a semi-insulating InP substrate. It consists of a 500 nm InAlAs buffer layer, a 15 nm InGaAs channel layer, a 3 nm InAlAs spacer layer, a 8 nm InAlAs barrier layer, and a 4 nm InP etching stopper layer. In order to achieve the good source and drain Ohmic contacts, the composite InGaAs cap layers with $3\text{x}10^{19}$ cm^{-2} silicon doping were applied. The Schottky gate contacts were formed by Ti/Pt/Au metallization and the Ohmic contacts were deposited using nonalloyed Ti/Pt/Au with 15/15/270 nm. The devices have a gate length of 120 nm and source-to-drain spacing of 2.4 μm. The gate width of two devices is 100 μm and 40 μm, respectively. The structure of device was shown in Figure 1 (a). The more detailed device fabrication process are shown in Figure 1 (b).

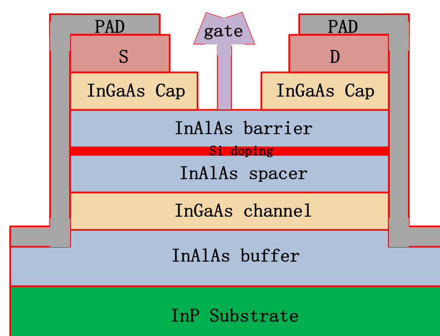

Fig. 1. The structure of InP-based HEMT.

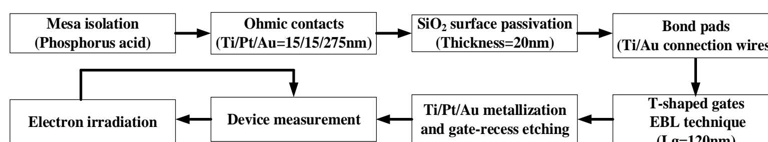

Fig. 2. The device fabrication process.

The InP-based HEMTs were irradiation at the Lanzhou Institute of Physics of China. The beam flux was about 1.33×10^{14} e/cm^2•s with a total dose up to 1×10^{16} cm^{-2} and the electron energy was 1 MeV, and all electrons were normal incidence on device. The DC and RF characteristics were measured by the B1500A semiconductor parameter analyzer and the E8363B PNA series vector network analyzer before and after electron irradiation at Zhengzhou University of China. The measured environment was at room temperature.

3. Results and discussion

The output characteristics (I_{DS}-V_{DS}) curves of InP-based HEMTs with different gate widths before and after electron irradiation were shown in Fig. 3 (a) and (b). The incident electron energy and dose were 1 MeV and 1×10^{16} cm^{-2}, respectively. The gate voltage (V_{GS}) ranged from 0 V to -0.6 V with a step of -0.1 V. It can be seen that the variation of drain current shown the similar degeneration trend after electron irradiation for different gate widths, as shown in Fig 3 (a). Specifically, saturation drain currents ($I_{D,\ sat}$) and specific channel on-resistance (R_{on}) are extracted from the I-V characteristics curves with different gate widths at $V_{GS} = 0$ V, as shown in Fig. 4. For device with 40 µm gate width, I_{Dsat} and R_{on} were decreased by 15.3% and 13.2%, respectively. For device with 100 µm gate width, I_{Dsat} and R_{on} were decreased by 13.8% and 10.2%, respectively.

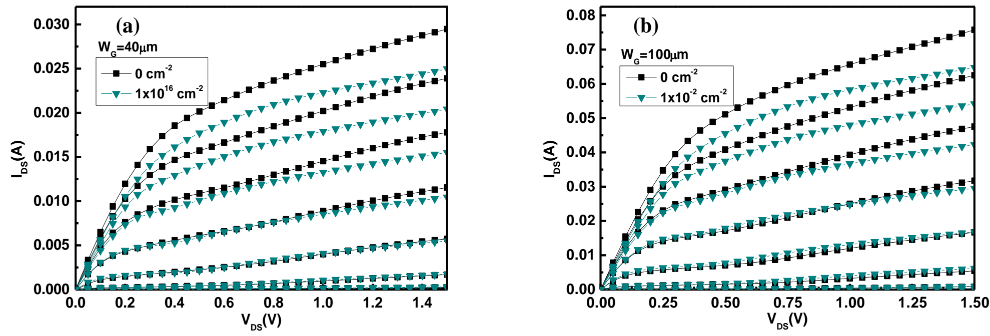

Fig. 3. I-V characteristics curves of InP-based HEMTs with different gate widths before and after electron irradiation, (a) 40 μm,(b) 100 μm.

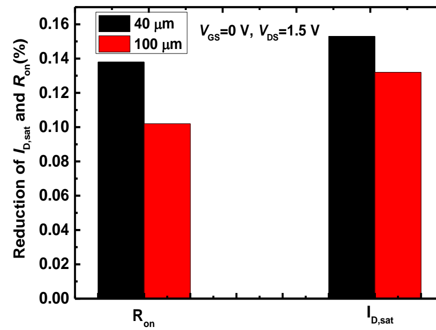

Fig. 4. The variation of the $I_{D,sat}$ and R_{on} at V_{GS} = 0 V with the different gate widths.

Figure 5 (a) and (b) described the transfer characteristics (I_{DS}-V_{GS}) of InP-based HEMTs with the gate width of 40 μm and 100 μm before and after 1×10^{16} cm^{-2} electron irradiation with V_{DS} =1.4 V at 1 MeV electron energy. The transconductance (g_m) and channel current (I_{DS}) of two kinds of devices were both decreased after electron irradiation. The variation of maximum transconductance ($g_{m,max}$) and the maximum channel current ($I_{D,max}$) were exactly computed from I_{DS}-V_{GS} curves for 40 μm and 100 μm devices, as shown in Fig. 6. For the device with 40 μm gate width, the $g_{m,max}$ and $I_{D,max}$ got dropped by 21.1% and 18.7% after electron irradiation, respectively. However, for the device with 100 μm gate width, the $g_{m,max}$ and $I_{D,max}$ got dropped by 18.1% and 12.9% after electron irradiation, respectively. Therefore, the device with large gate width had a stronger radiation resistance.

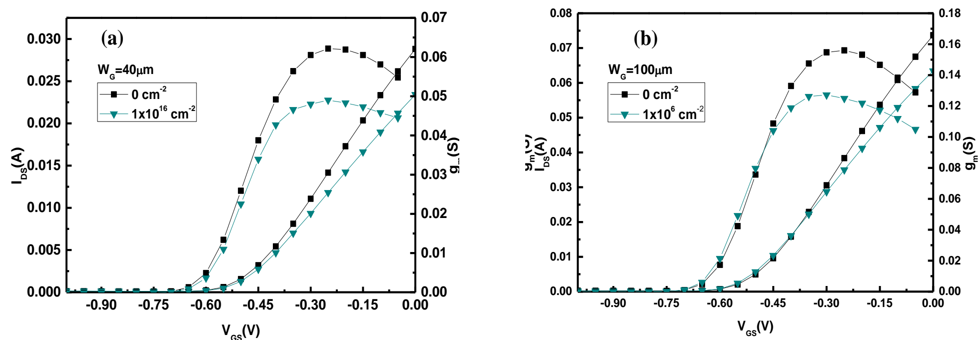

Fig. 5. Transfer characteristics curves of InP-based HEMTs with different gate widths before and after electron irradiation, (a) 40 μm,(b) 100 μm.

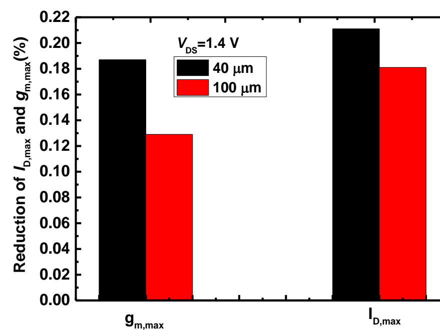

Fig. 6. The variation of the $I_{D,sat}$ and R_{on} at V_{DS} = 1.4 V with the different gate widths.

The defects induced by electron irradiation in the hetero-junction region degenerated the electron density and mobility through the carrier removal effect and scattering effect and led to the degeneration of output and transfer characteristics of device. To understand the irradiation-induced charged defects on the electron density and mobility, the electron density and mobility were calculated by[19-21]:

$$n_s = \frac{\varepsilon}{qd}\left(V_{GS} - V_{TH}\right), \quad \mu_{channel} = \frac{L}{WC_{OX}V_{DS}} g_m$$

where V_{TH} is the threshold voltage, L and W are the gate length width, n_s is sheet electron concentration, $\mu_{channel}$ is electron mobility in the channel. Form the I_{DS}-V_{GS} curves, the values of V_{TH} for the devices with 40 μm and 100 μm gate width were almost unchanged after electron irradiation. Therefore, the electron concentrations calculated by above equation were shown nearly invariable after electron irradiation for devices with different gate width. However, the values of $\mu_{channel}$ calculated by above equation for the devices with 40 μm and 100 μm gate width were reduced by 78.9% and 67.9% after electron irradiation, respectively. In addition, the $\mu_{channel}$ of device with small gate width was reduced more seriously than the device with large gate width. Hence, the degeneration of output and transfer characteristics of InP based HEMTs by electron irradiation were mainly attributed to the decreased $\mu_{channel}$ after electron irradiation and the device with small gate width was degenerated more severely. The defects distributions under the gate induced by electron irradiation were more concentrated at the small gate width and resulted in the more stronger scattering effect than the large gate width. Moreover, the surface morphology of small gate width become more rough after electron irradiation. Therefore, the characteristics of device with 40 μm gate width showed the more serious degeneration.

The forward gate current curves of InP-based HEMTs with different gate width were shown in Fig. 7 (a) and (b). After electron irradiation, the forward current got decreased for both device, and the device with 40 μm gate width was reduced more significantly. This was mainly due to the increase of series resistance after electron irradiation. The series resistance can be extracted from slop of dV/d(LnI)-I curves at forward bias condition, and was calculated by[22]: $\frac{dV}{d(\ln I)} = R_s I + \frac{nkT}{q}$. Figure 8 shows the dV/d(LnI)-I curves of both devices before and after electron irradiation. It can be seen that the slope of curves were both increased after electron irradiation, which meaned the resistance went up. The series resistance was increased from 4.9 Ω to 7.1 Ω for device with 40 μm gate width, and the series resistance was increased from 4.6 Ω to

5.1 Ω for device with 100 μm gate width. Hence, the forward current of device with 40 μm gate width was degenerated more severely.

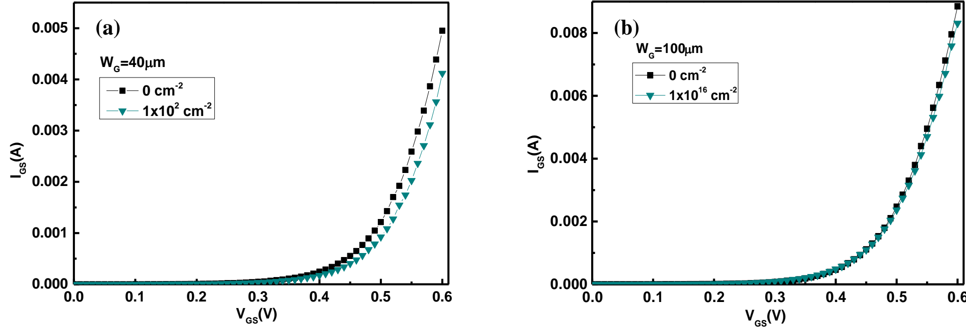

Fig. 7. Forward gate current curves of InP-based HEMTs with different gate widths before and after electron irradiation, (a) 40 μm,(b) 100 μm.

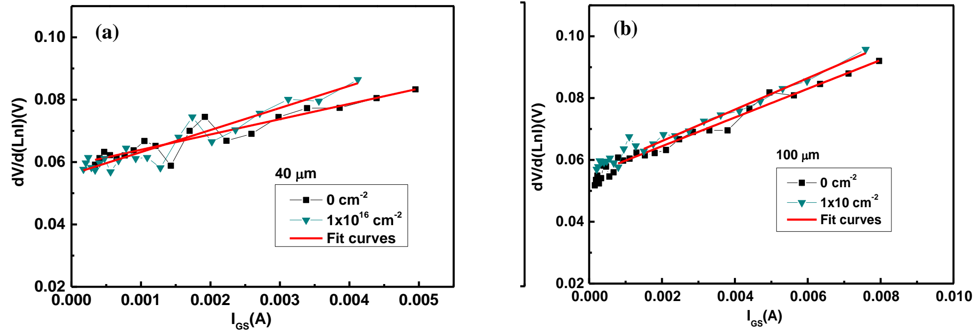

Fig. 8. dV/d(LnI)-I curves of both device before and after electron irradiation, (a) 40 μm,(b) 100 μm.

The ideality factor and the Schottky barrier height are main parameters for gate-characteristics of InP-based HEMTs. According to the thermionic-emission model, the ideality factor and the Schottky barrier height can be obtained from the slope and intercept of Ln I-V plot, the equations can be written as: [23-25]

$$n = \frac{q}{kT}\left(\frac{dV}{d\ln I}\right), \quad \Phi_B = \frac{kT}{q}\ln\left(\frac{SA^{*}T^{2}}{I_{s0}}\right)$$

where, S is the contact area, A^* is the effective Richardson constant,14.4 A/cm^2*K, q is the electronic charge, k is the Boltzman constant, T is absolute temperature, V is the applied voltage across the structure, I_{S0} is the reverse saturation current, n and Φ_B are the ideality factor and the Schottky barrier height, respectively. The n was increase by 4.3% and 12.2% for device with 40 and 100 μm gate width, respectively. However, Φ_B had a little change for both devices. The interface states introduced by electron irradiation could be considered to be the reason for the change of n[24,25].

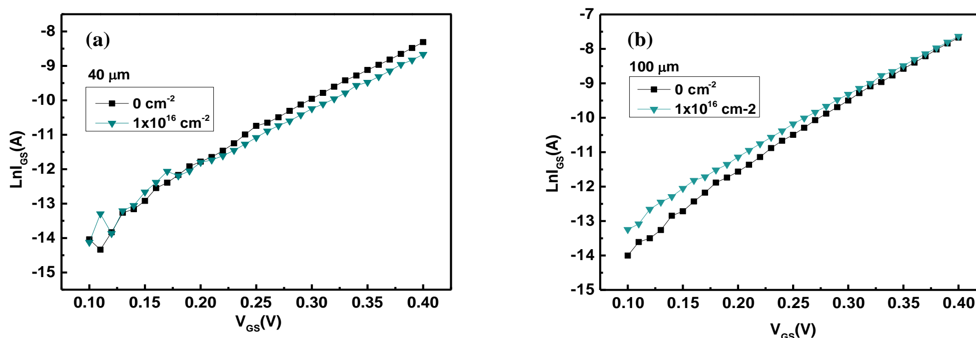

Fig. 9. Semi-log plot of the I_{GS}-V_{GS} curves before and after electron irradiation at line region, (a) 40 μm,(b) 100 μm.

Figure 10 (a) and (b) showed the reverse gate current characteristics of InP-based HEMTs with different gate width before and after electron irradiation. After electron irradiation, the reverse gate current of the devices with different gate width were both increased, and the reverse gate current was deteriorated more worse for devices with different 40 μm gate width. Under the reverse bias, the Fermi level of semiconductor material at the interface might be below the defect level and lead to the defects release electrons. Therefore, the number of electrons passing through the Schottky barrier will be increased, and the reverse gate current will be enhanced with larger radiation fluence[26].

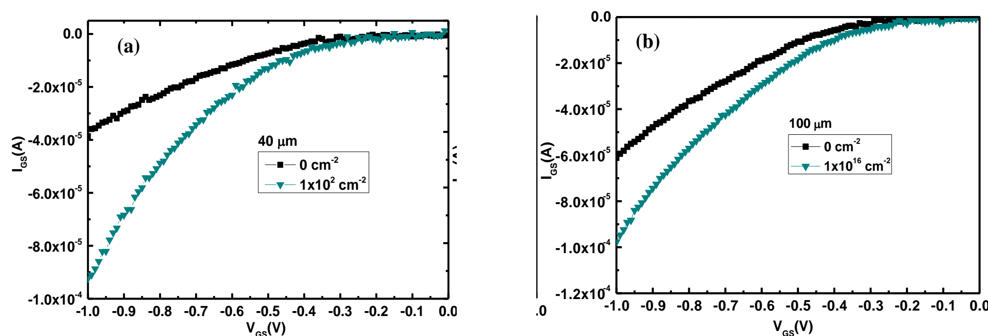

Fig. 10. Reverse gate current curves of InP-based HEMTs with different gate widths before and after electron irradiation, (a) 40 μm,(b) 100 μm.

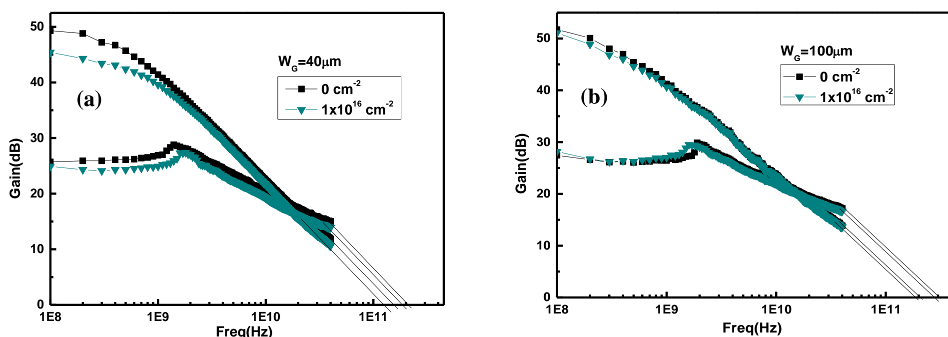

Fig.11. Frequency characteristics of InP-based HEMTs before and after electron irradiation with different gate widths, (a) 40 μm,(b) 100 μm.

Figure 11 shows f_T and f_{max} of InP-based HEMTs before and after electron irradiation. After electron irradiation, both f_T and f_{max} demonstrated a downward trend. The defects induced by electron irradiation increased the gate-drain capacitance and the specific channel on-resistance and led to the degeneration of f_T and f_{max}[20]. For device with 40 μm gate width, the f_T was decreased from 153.0 GHz to 122.7 GHz and f_{max} was decreased from 208.5 GHz to 185.7 GHz. The f_T and f_{max} were reduced by 19.8% and 10.9%, respectively. For device with 100 μm gate width, the f_T was decreased from 139.4 GHz to 125.5 GHz and f_{max} was decreased from 226.2 GHz to 206.1 GHz. The f_T and f_{max} were reduced by 7.1% and 8.2%, respectively. Therefore, the InP-based HEMT device with large gate width demonstrates a good capability when it works in an irradiation environment.

4. Conclusions

In conclusion, the effects of electron irradiation on DC and RF characteristics of InP-based HEMTs with different gate width are investigated. After electron irradiation, the I_{DS} and g_m were both reduced for device with different gate width. The reduction of carrier mobility in the channel was the reason for degeneration I_{DS} and g_m. Meanwhile, the f_T and f_{max} were also decreased after electron irradiation, which was mainly due to the increase of gate-drain capacitance and specific channel on-resistance after electron irradiation. Additionally, the increase of series resistance caused by electron irradiation was led to the reduction of forward gate current, and the value of reverse gate leakage current increased after electron irradiation, which can be accounted for the increased electrons released by the induced defects under reverse bias. Although the DC and RF characteristics of both devices were degenerated induced by electron irradiation, the device with large gate with was demonstrated to strongly resist to irradiation.

Acknowledgements

This research was funded by the National Natural Science Foundation of China (No.11775191, 61973177), Natural Science Foundation of Henan Province (Grant No. 202300410379, 202300410281), Promotion Funding for Excellent Young Backbone Teacher of Henan Province in China (2019GGJS017), Promotion Project for Physics Discipline in Zhengzhou University of China (2018WLTJ01), Henan International Joint Laboratory of Behavior Optimization Control for Smart Robots, file No. [2018]19, National Scientific Research Project Cultivation Fund of Huanghuai University (No. XKPY-202103, XKPY-202106, XKPY-202006), Young Backbone Teachers of Huanghuai University. Key Scientific Research Projects of Colleges and Universities in Henan Province (No.21B140006), the Science and Technology Project in Henan Province (No.212102310905, 212102210516).

References

[1] B. A. Floyd, S. K. Reynolds, U. R. Pfeiffer T. Zwick, T. Beukema, B. Gaucher, IEEE J. Solid-St. Circ. **40**, 156 (2005).

[2] W. Li, R. Kraemer, J. Borngraeber, in IEEE MTT-S International Microwave Symposium Digest, 1834 (2006).

[3] D. R. Vizard, R. Doyle, in IEEE MTT-S International Microwave Symposium Digest, 94 (2006).

[4] C. Zhao, B. Xu, J. Z. Wang, Z. G. Wang, J. Semicond. **41**, 011103 (2020).

[5] S. X. Sun, B Yang, Y. H. Zhong, Y. X. Li, P. Ding, Z. Jin, Z. C.Wei, J. Phys. D: Appl. Phys. **53**, 175107 (2020).

[6] S. X. Sun, Y. H. Zhong, H. Y. Mei, R. X. Yao, F. J. Chen, Y. X. Li, Y. F. Hu, Journal of Ovonic Research **17**, 137 (2021).

[7] J. Ajayan, D. Nirmal, T. Ravichandran , P. Mohankumar, P. Prajoon, L. Arivazhagan, S. C. Kumar, Int. J. Electron. Commun. (AEÜ) **94**, 199 (2018).

[8] Y. H. Zhong, K. K. Li, M. K. Li, W. B. Wang, S. X. Sun, H. L. Ma, P. Ding, Z. Jin, J. Infrared. Millim. W. **37**, 171 (2018).

[9] Y. H. Zhong, B. Yang, M. M. Chang, P. Ding, L. H. Ma, M. K. Li, Z. Y. Duan, J. Yang, Z. Jin, Z. C. Wei, Chin. Phys. B **29**, 038502 (2020).

[10] Ajayan, D. Nirmal, J. Semicond. **88**, 044001 (2017).

[11] A. Y. Polyakov, S. J. Pearton, P. Frenzer, R. Fan, L. Lu, J. Kim, J. Mater. Chem. C **1**, 877 (2015).

[12] S. Sun, M. Chang, C. Zhang, C. Chao, Y. H. Zhong, Y. X. Li, P. Ding, Z. Jin, Z. C. Wei, Phys. Status Solidi RRL **6**, 1800027 (2018).

[13] S. J. Pearton, R. Deist, F. Ren, L. Liu, A. Y. Polyakov, J. Kim, J. Vac. Sci. Technol. A **31**, 050801 (2013).

[14] E. A. Douglas, E. Bielejec, P Frenzer, B. R. Yates, S. J. Pearton, C. F. Lo, L. Liu, T. S. Kang, F. Ren, J. Vac. Sci. Technol. B **31**, 021205 (2013).

[15] L. Lv, J. G. Ma, Y. R. Cao, J. C. Zhang, W. Zhang, L. Li, S. R. Xu, X. H. Ma, X. T. Ren, Y. Hao, Microelectron. Reliab. **51**, 2168 (2011).

[16] L. Liu, V. C. Cuervo, Y. Xi, F. Ren, J. Vac. Sci. Technol. B **31**, 042202 (2013).

[17] T. Kimura, R. Shigemasa, T. Ohshima, Solid State Electron. **41**, 1457 (1997).

[18] S. Li, Y. H. Hwang, Yu. L. Hsieh, L. Lei, F. Ren, S. J. Pearton, E. Patick, M. E. Law, C. V. Cuervo, D. J. Smith, J. Vac. Sci. Technol. B **32**, 021203 (2014).

[19] X. W. Hu, P. K. Aditya, B. Jun, D. M. Fleetwood, R. D. Schrimpf, R. D. Geil, R. A. Weller, B. White, M. Bataiev, IEEE Trans. Nucl. Sci. **50**, 1791 (2003).

[20] S. X. Sun, P. Ding, Z. Jin, Y. H. Zhong, Y. X. Li, Z. C. Wei, Nanomaterials **9**, 967 (2019).

[21] F. Chen, W. X. Tang, G. H. Yu, L. Zhang, B. S. Zhang, Acta Physica Sinica **69**, 098501 (2020).

[22] N. Hamdaoui, R. Ajjel, B. Salem, M. Gendry, Mat. Sci. Semicon. Proc. **26**, 431 (2014).

[23] I. P. Vali, P. K. Shetty, M. G. Mahesha, V. C. Petwal, J. Dwivedi, R. J. Choudhary, Appl. Surf. Sci. **407**, 171 (2017).

[24] A. Chatterjee, S. K. Khamari, S. Porwal, S. Kher, T. K. Sharma, J. Appl. Phys. **123**, 161585 (2018).

[25] N. Shiwakoti, A. Bobby, K. Asokan, B. Antony, Mat. Sci. Semicon. Proc. **74**, 1 (2018).
[26] V. Baranwal, S. Kumar, A. C. Pandey, D. Kanjilal, J. Alloy. Compd. **480**, 962 (2009).